Steady to unsteady dynamics of a vesicle in a flow

J. Beaucourt, F. Rioual, T. Séon, T. Biben, and C. Misbah
Groupe de Recherche sur les Phénomènes Hors Equilibre, LSP, Université Joseph Fourier, CNRS UMR No. 5588, Boîte Postal 87, F-38402 Saint Martin d'Hères Cedex, France
(Received 1 July 2003; published 26 January 2004)

We investigate the dynamics of a vesicle in a shear flow on the basis of the newly proposed advected field (AF) method [T. Biben and C. Misbah, Eur. Phys. J. E **67**, 031908 (2003)]. We also solve the same problem with the boundary integral formulation for the sake of comparison. We find that the AF results presented previously overestimated the tumbling threshold due to the finite size of the membrane, inherent to the AF model. A comparison between the two methods shows that only in the sharp interface limit (extrapolating the results to a vanishing width) the AF method leads to accurate quantitative results. We extensively investigate the tank-treading to tumbling transition, and compare our numerical results to the theory of Keller and Skalak which assumes a fixed ellipsoidal shape for the vesicle. We show that this theory describes correctly the two regimes, at least in two dimensions, even for the quite elongated non-convex shapes corresponding to red blood cells (and therefore far from ellipsoidal), This theory is, however, not fully quantitative. Finally we investigate the effect of a confinement on the tank-treading to tumbling transition, and show that the tumbling regime becomes unfavorable in a capillary vessel, which should have strong effects on blood rheology in confined geometries.

DOI: 10.1103/PhysRevE.69.011906 PACS number(s): 87.16.Dg, 47.60.+i, 87.17.Jj

A vesicle is a closed phospholipid membrane, separating an internal fluid from the external suspending medium. The size of a vesicle can vary in quite a broad range from a few tens of nanometers, in which case they are called liposomes, up to a hundred microns, where they are named giant vesicles. The shape of these vesicles strongly depends on the swelling ratio τ, which expresses the volume/surface ratio in a dimensionless form $\tau=6\sqrt{\pi}V/S^{3/2}$, where V denotes the internal volume of the vesicle and S its area. While a spherical shape corresponds to $\tau=1$, τ can vary in practice between 0 and 1, and give rise to a large variety of equilibrium shapes as studied after the seminal works by Canham, Helfrich, and Evans [1–3] by many authors since [4–8]. Among the variety of observed shapes is the oblate shape, for $0.592<\tau<0.651$, and the stomatocyte shape for $\tau<0.592$ (after Ref. [5]), which coincide with the usual equilibrium shapes of red blood cells. Since giant vesicles can be as large as 100 μm, their properties can be investigated using standard optical microscopy techniques, and constitute, therefore, in view of their conceptual simplicity, a theoretical and experimental model system for blood flows. Of course there is no common point between a red blood cell and a vesicle from the biological point of view; a vesicle only contains phospholipids, a major ingredient of cell membranes, but has no biological function. Interestingly, it should be possible to incorporate more complicated, and biologically relevant, ingredients like proteins to the phospholipid membrane to selectively activate some biochemical properties. Equivalently, the encapsulated fluid could be modified to mimic in a more realistic way the internal medium of a red blood cell. It is, however, not our purpose here to model the biological properties of a red blood cell. Rather we will focus on their mechanical properties. Understanding blood rheology is a major issue for biomedical applications. At the macroscopic scale blood is a non-Newtonian fluid (see, e.g., Ref. [9]), and a precise knowledge of its flowing properties is necessary to understand some pathologies, or to design artificial devices. Since blood properties are very sensitive to experimental conditions, a special effort is made to find blood analogs, mimicking their rheological properties without the biological complications. At a more microscopic scale, blood is responsible for cell transport and can then play an active role in the propagation of some pathologies, like cancer for example. Mechanical models have then been suggested to describe the dynamic of a red blood cell in an external flow, like the ''capsule'' model, which aims at a quantitative description of red blood cell flows. These models include elastic properties of the red blood cell membrane (see, e.g., Refs. [10–15]). Our scope here is different; instead of including all the relevant physical ingredients necessary to derive a quantitative description of blood flows, which is certainly of very important practical interest, but unfortunately often shadows simple, but important physical mechanisms, we want to identify these elementary mechanisms by including a minimal set of physical ingredients on the contrary. More realistic models can then be constructed step by step, isolating the influence of each physical ingredient at a time. From this point of view, a vesicle constitutes the ideal starting point for this kind of approach, since its equilibrium properties depend on the swelling factor τ and the area difference between the internal and external monolayers, and its dynamical properties are controlled by a very small set of dimensionless numbers, two in the simplest approach and three when a viscosity contrast between the encapsulated fluid and the external medium is accounted for. In this paper we shall keep the analysis rather simple by disregarding the area difference between the monolayers, though we are aware of the importance of this ingredient with regard to equilibrium shapes. The key simplification comes from the liquid nature of the membrane. It shares the same inextensibility property with red blood cell, which is certainly the reason for the success of this naive model, but there is no shear modulus, in contrast with

 ©2004 The American Physical Society

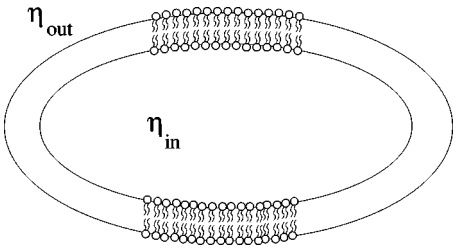

FIG. 1. Schematic drawing of a vesicle.

red blood cells for which a weak shear modulus is revealed. This is indeed a great simplification since accounting for shear elasticity raises the problem of the tensionless reference surface, which is unknown for red blood cells, and strongly affects the results [15]. The vesicle model suppresses this difficulty, rendering an interpretation of the results much simpler. Moreover, although very simplistic, the vesicle model seems to be qualitatively, but also semiquantitatively, quite reliable to describe the physical effects observed in blood flows. In this paper we present a quantitative numerical study of the tank-treading to tumbling transition in vesicular systems, and show that the Keller-Skalak (KS) theory [16], based on fixed ellipsoidal shapes, correctly describes the transition mechanism, even for highly nonellipsoidal shapes in two dimensions. This transition between a steady regime and a nonsteady tumbling motion is indeed of fundamental importance in blood since it strongly affects its rheological properties [9]. Moreover we show that a confinement of the vesicle between two rigid walls shifts the location of the transition, which should have consequences on the rheological properties of blood in capillary vessels.

In Sec. I we present the model, the parameters and the general equations. The numerical techniques we used to solve the hydrodynamic free boundary problem are presented in Appendixes A, B and C, where we revisit the newly proposed advected field (AF) method [17], and analyze the sensitivity of the method to internal parameters. In Sec. II we compare the numerical results to the KS theory, and analyze the dissipation in Sec. III. Section IV is devoted to confinement, and a discussion with some open questions is presented in Sec. V. Some technical calculations are relegated to the Appendixes.

I. MODEL AND EQUATIONS

A. Model

A vesicle is a closed phospholipid membrane as depicted in Fig. 1, ideally a bilayer, but sometimes a multilayer membrane. Depending on temperature, and the chemical nature of the surfactants, the molecular organization of the membrane can be of the liquid type, or correspond to a crystal, or even form a gel-like structure. At a mesoscopic scale, the mechanical properties of the membrane can then vary from a two-dimensional liquid to an elastic solid. In any case, the extensibility of the membrane is very low, and it is usually assumed to be inextensible; we will use this assumption here. The other possible in-plane deformation is a shear. If the membrane is purely liquid, as we will assume here, this distortion does not cost any energy, whereas if the membrane is elastic (as red blood cells are) it will store elastic energy. For a liquid inextensible membrane, the only energetic contribution is then in out of plane deformations, which are essentially bending modes. Several models have been considered for the membrane energy, starting from the simplest model suggested by Helfrich [2],

$$E_H=\frac{\kappa}{2}\int (c_1+c_2)^2 dS+\frac{\overline{\kappa}}{2}\int c_1c_2 dS, \tag{1}$$

where c_1 and c_2 are the two main curvatures, in three dimensions, at a given point of the membrane. The total curvature c_1+c_2 and the Gaussian curvature c_1c_2 are the two geometrical invariants characterizing the surface at a given point. Since curvatures are algebraic, and physical properties of the membrane do not depend on the precise sign of these quantities if the membrane is symmetrical, the energy should be quadratic. Integrals are calculated over the surface of the membrane. κ and $\overline{\kappa}$ are the elastic moduli characterizing the two possible deformation modes, and we have assumed that the membrane is homogeneous to extract them from the integrals. Thanks to the Gauss-Bonnet theorem the Gaussian contribution is a constant that only depends on the topology. When the vesicle is not subjected to topological changes (like budding for example) $\overline{\kappa}$ does not play any role. We will accordingly disregard the Gaussian contribution from the energy in the following. When minimizing the energy, the constraint of local inextensibility of the membrane have to be accounted for, using for example a local Lagrange's parameter $\zeta(s,t)$ which is a function of the arclength (and of time in dynamical regimes):

$$E=E_H+\int \zeta(s,t)dS.$$

A minimization of the total energy can be performed to compute the equilibrium shapes of the vesicle. Interestingly, the Helfrich formulation is scale invariant, which means that the typical size of the vesicle does not play any role. The only relevant parameter is the swelling ratio $\tau=6\sqrt{\pi}V/S^{3/2}$, where V is the volume of the vesicle and S its area ($\tau=4\pi S/P^2$ in two dimensions where P is the perimeter of the vesicle). When a flow is applied, hydrodynamical quantities will enter into play, which will be considered now.

B. Hydrodynamical equations

Since the typical size of a vesicle is of the order of 10 μm, and typical shear rates applied to these vesicles are usually smaller than 10 Hz, the Reynolds number can be estimated to be of the order of 10^{-3} in water. Inertial effects are then negligible and the appropriate equation to describe the hydrodynamic flow inside and outside the vesicle is the Stokes equation

$$\nabla\cdot\sigma-\nabla p+\mathbf{f}_{ext}=0, \tag{2}$$

where $\sigma=\eta(\nabla\mathbf{v}+\nabla\mathbf{v}^T)$ is the Newtonian stress tensor (notation T denotes a transposition of the gradient velocity ten-

sor), η is the viscosity of the considered medium [for water $\eta = 1.0 \times 10^{-2}$ P at 20° C (g cm^{-1} s^{-1})], $\mathbf{v}$ is the velocity field, p is the pressure field and $\mathbf{f}_{ext}$ is the local force exerted by external objects, like the vesicle itself and eventually a substrate, on the fluid. Finally, the liquid is incompressible for all practical purposes, entailing that:

$$\nabla \cdot \mathbf{v} = 0. \tag{3}$$

The contribution of the vesicle to the external force can be derived from its configurational Hamiltonian

$$E = \frac{\kappa}{2} \int c^2 ds + \int \zeta(s) ds, \tag{4}$$

where we recognize the curvature energy (the first term) corresponding to the Helfrich theory [2], c is the local curvature of the membrane $c = c_1 + c_2$ and s denotes the coordinates along the membrane (the curvilinear coordinate along the contour of the vesicle in two-dimensions), κ is the curvature rigidity, and the second term expresses the constraint of fixed perimeter. $\zeta(s)$ is a local Lagrange's parameter expressing the absence of local dilatation of the membrane. The force field exerted by the vesicle on the flow is simply given by $\mathbf{f}_{ext} = -\delta E / \delta \mathbf{R}$, where $\delta \mathbf{R}$ is a local elementary translation of the membrane forming the vesicle.

The last prescription needed to derive the dynamical equations for the vesicle is the boundary condition for the velocity field at the membrane. The simplest prescription compatible with the absence of permeation is to assume that the vesicle is purely advected (transported) by the flow, which means that the local velocity of the membrane is the local velocity of the flow:

$$\mathbf{v}_{mem} = \mathbf{v}. \tag{5}$$

The final set of equations is then

$$\nabla \cdot \sigma - \nabla p + \mathbf{f}_{ext} = \mathbf{0},$$

$$\nabla \cdot \mathbf{v} = \mathbf{0},$$

$$\mathbf{f}_{ext} = -\frac{\delta E}{\delta \mathbf{R}},$$

$$\mathbf{v}_{mem} = \mathbf{v}. \tag{6}$$

These equations have to be solved numerically, and we will consider both the boundary integral method (Appendix A) and the AF method (Appendix B). A comparison between the two methods is the subject of Appendix C. We will mostly use the boundary integral method for quantitative comparisons with the KS theory (Sec. II) and the AF method for qualitative discussions (Sec. III). We will now more specifically consider the two-dimensional (2D) geometry.

C. Relevant parameters

The first relevant parameter is the swelling ratio τ that controls the equilibrium shape of the vesicle. The relaxation time of the shape of the vesicle is controlled by the viscosity of the fluid; a typical relaxation time can be constructed as $t_{shape} = \eta R^3 / \kappa$, where η is a viscosity. We take the viscosity of the external fluid to define various quantities of physical interest, and it will be denoted η_{out} (while η_{in} refers to that of the liquid inside the vesicle). The typical temporal scale of the shape evolution is $t_{shape} = \eta_{out} R^3 / \kappa$, where R is a length scale which we will choose as $R = \sqrt{S/\pi}$ in two dimensions, the radius of the disk of the same area. Indeed, these definitions based on dimensional considerations do only provide orders of magnitude, as long as the viscosity ratio is not too large ($\leqslant 10$) the replacement of η_{in} by η_{out} will not change the overall picture. In the presence of a shear flow, the shear rate γ defines a time scale $1/\gamma$ and therefore, combined to t_{shape} we can construct the dimensionless number $C_\kappa = \eta_{out} \gamma R^3 / \kappa$ which characterizes the deformability of the vesicle under the hydrodynamic constraint γ. The larger C_κ is, the larger the deformation due to the flow. When allowance is made for a viscosity contrast between the internal fluid and the suspending medium, the viscosity ratio $r = \eta_{in} / \eta_{out}$ will also come into play. To summarize, the three relevant parameters in the problem are

$$\tau = 4\pi S / P^2 \quad \text{in two dimensions,}$$

$$C_\kappa = \eta_{out} \gamma R^3 / \kappa,$$

$$r = \eta_{in} / \eta_{out}.$$

II. TEST OF THE KS THEORY

A shear flow can be viewed as the superposition of a pure rotational flow and an elongational flow which main elongation axis is oriented at 45 from the shear direction. That is we can write a simple shear $\mathbf{v} = (\gamma y, 0)$ as

$$\mathbf{v} = M_s \mathbf{r} + M_a \mathbf{r}, \tag{7}$$

where M_s (with components $M_s^{xx} = M_s^{yy} = 0$ and $M_s^{xy} = M_s^{yx} = \gamma/2$) is a traceless symmetric matrix (describing the straining of the vesicle along $\pi/4$), while M_a (with components $M_a^{xx} = M_a^{yy} = 0$ and $M_a^{xy} = \gamma/2$ and $M_a^{yx} = -\gamma/2$) is a traceless antisymmetric matrix, representing the rotational part of the flow.

When an object is placed in such a flow it experiences a torque inducted by the rotational component of the velocity field, and a torque due to the elongational part which tends to orient the particle at 45 from the shear direction. The resulting motion of the particle depends on the competition between these two components of the flow, and the generic evolution equation for the orientation θ of a particle is of the form

$$\frac{d\theta}{dt} = A + B \cos(2\theta), \tag{8}$$

where A and B are two coefficients characterizing the competition. Of course, all the complexity of the problem lies in the determination of these coefficients in a particular situation, but Eq. (8) shows that basically two regimes are possible: when $|A/B| < 1$ a steady state can exist, and the orien-

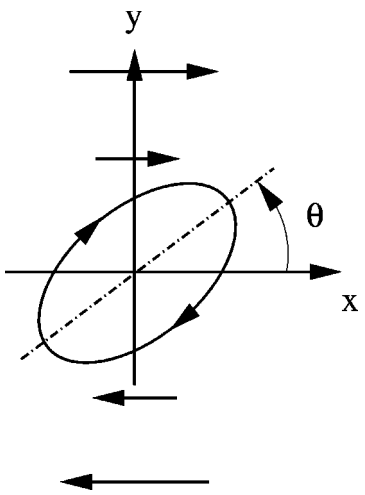

FIG. 2. schematic drawing of a tank-treading vesicle in a simple shear flow.

tation is given by $\cos(2\theta)=-A/B$ (the tank-treading regime), and when $|A/B|>1$ the motion cannot be stationary and the particle rotates in the flow (the tumbling regime). Two branches exist in the tank-treading regime corresponding to $\theta=\pm\arccos(-A/B)/2$. With the conventions of Fig. 2, $\theta>0$ corresponds to the stable branch while $\theta<0$ is unstable. The two branches meet at $\theta=0$, which corresponds to the limit of stability. When $|A/B|$ is varied from 0 to infinity, the orientation θ varies from 45 degrees to zero, reached for $|A/B|=1$, and a transition to a tumbling motion occurs for larger values. In the terminology of the bifurcation theory, this kind of transition is called a saddle-node bifurcation. In their paper, Keller and Skalak were able to derive expressions for A and B on the basis of Jeffery's work on rigid ellipsoids [18], and they applied their theory to the special case of red blood cells. In view of the importance of this tank-treading to tumbling transition for blood rheology, it seems interesting to compare this theory numerically to the full free boundary resolution. Since the deformability of the particle is not taken into account in the KS theory, we chose to consider the regime $C_\kappa<1$ which corresponds to weakly deformable vesicles. We checked that in practice the precise value of C_κ does not affect the results much, as shown in Fig. 3 for a

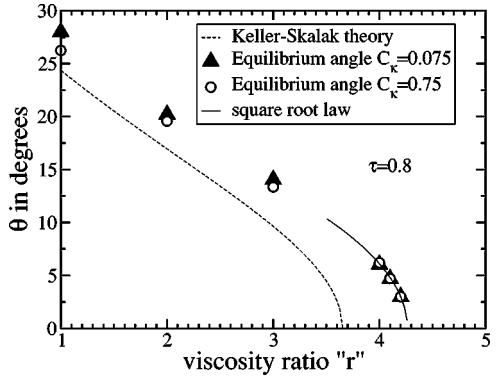

FIG. 3. Orientation angle (in degrees) as a function of the viscosity ratio for $\tau=0.8$ and two values of C_κ.

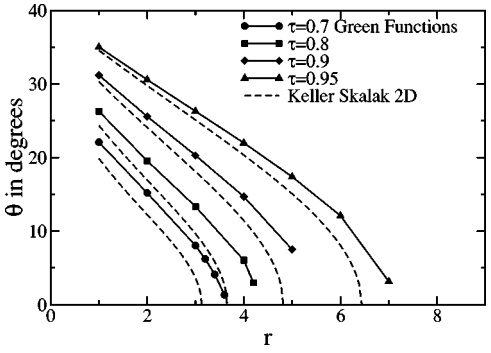

FIG. 4. Orientation angle as a function of the viscosity ratio for various values of the swelling ratio.

swelling ratio $\tau=0.8$. In this figure we plot the variations of the equilibrium angle θ as a function of the viscosity ratio r for two different values of C_κ (0.75 and 0.075). We observe a variation only close to $r=1$ which remains far away from the transition. This lack of sensitivity is very interesting since it means that the constraints of fixed perimeter and area (surface and volume in three dimensions) are playing the leading role, and the precise value of κ, the curvature modulus, is not very important in the $C_\kappa<1$ regime. This property is very interesting from an experimental point of view, since usually κ is difficult to measure. The dynamical situation is then quite similar to the equilibrium situation (no flow), for which κ can rigorously be eliminated from the problem. The only relevant parameters are thus τ and r, the viscosity ratio. Close to the transition, the KS theory predicts a square root dependence of the orientation angle θ as a function of r [A/B is linear in r and $\theta=\arccos(-A/B)/2$, once linearized around $-A/B\sim1$ leads to a square root law]. This square root law is represented in Fig. 3 and is seen to be fairly well reproduced. Indeed, an extrapolation to $\theta=0$ of this square root fit is a powerful way of measuring the critical viscosity ratio r_c. The quantitative comparison with the KS theory exhibits some discrepancies, this theory tends to slightly underestimate the critical viscosity ratio r_c. A more systematic study is presented in Fig. 4, where we can see the variations of the main axis orientation θ as a function of the viscosity ratio for various values of the reduced surface τ.

In this figure the dashed lines correspond to the KS theory in two dimensions, while the simulation data using the integral method are represented by the symbols. We can see that, although the KS theory captures the generic scenario of the transition, still some quantitative discrepancies exist between the theory and the numerical results: the critical viscosity ratios are a bit underestimated by the theory. Interestingly, the difference between the theory and the numerical data does not seem to be very sensitive to the swelling ratio τ, although it could be expected to be larger for low values of τ for which the equilibrium shapes are far from ellipsoidal. A final comparison between the KS theory and the numerical free boundary resolution is seen in Fig. 5, where the KS predictions for r_c are confronted to both the AF results and the boundary integral resolution. We basically observe the same trend as already mentioned. Amazingly, the free boundary numerical resolution in two dimensions seems to be

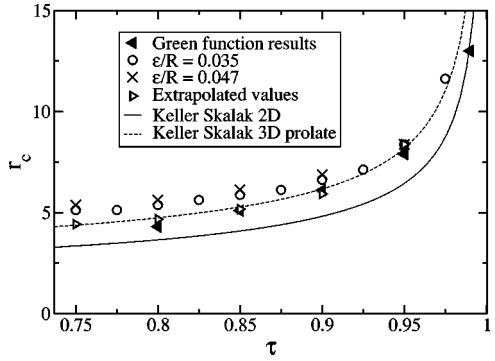

FIG. 5. Tank-treading to tumbling transition curve. Here we compare the AF data, the Green function formulation, and the KS theory. Two values of ϵ are plotted for the AF method and the extrapolated $\epsilon=0$ (see Appendix C) value superimposes quite well on those obtained using the boundary integral formulation.

closer to the 3D KS predictions for a prolate shape than the 2D expectations, but this is probably purely accidental.

III. ANALYSIS OF THE TRANSITION WITHIN THE AF APPROACH

Stationary states result from a balance between the energy flux entering in the system and the hydrodynamic dissipation. From this general consideration it is, for example, easy to extract the main dependences of the Stokes drag force acting on a sphere moving at velocity v in a viscous fluid: the injected energy is simply Fv, where F is the force exerted on the sphere to compensate for the Stokes force; the dissipation rate is given by

$$\dot{E}_{hydro}=\int \frac{\eta}{2}\left(\frac{\partial v_i}{\partial x_j}+\frac{\partial v_j}{\partial x_i}\right)^2 dV, \tag{9}$$

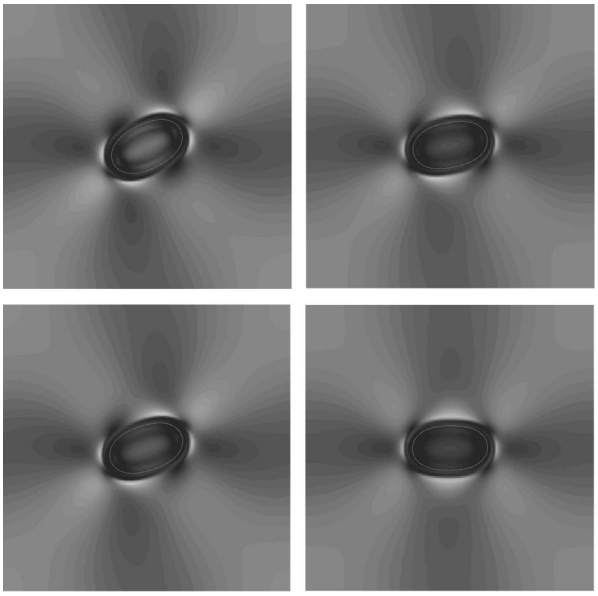

FIG. 6. Dissipation field around the vesicle for $\tau=0.91$ and, from right to left and top to bottom, $r=2$, 4, 6, and 7.8, close to r_c ($\epsilon/R=0.068$). White areas are places where dissipation is maximal. The line indicates the $\phi=0$ isocontour of the AF.

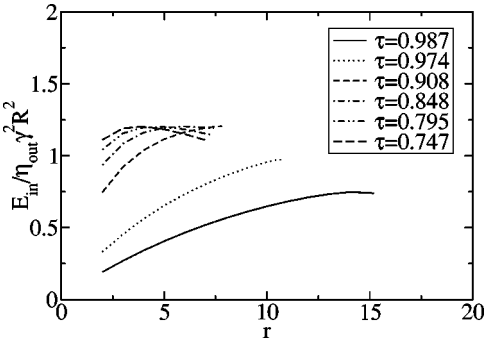

FIG. 7. Internal dissipation rate as a function of the viscosity ratio.

where the integration covers the volume where dissipation occurs. If we assume that the range of the flow perturbation due to the sphere is proportional to its radius R, replacing ∇v by v/R and the volume integration by $\times R^3$ we recover the classical dependencies of the Stokes force, namely, $F \propto \eta v R$. This kind of heuristic analysis can be powerful when the typical scales are well defined. Conversely, when several length scales compete such arguments require a more quantitative analysis. This is indeed the case here where the swelling ratio τ, which is directly connected to the ratio between the large and the small axis of the vesicle, plays a key role. We thus have to analyze dissipation in more details.

In Fig. 6 we present isocontour plots of the dissipation field for a vesicle of reduced surface $\tau=0.91$ and for different viscosity ratios, $\eta_{in}/\eta_{out}=2.0$, 4.0, 6.0, and 7.8 [close to the tumbling transition for ($\epsilon/R=0.068$)]. We can see that dissipation is localized in a very narrow area *outside* the vesicle, we also see contributions along the diagonal axis due to the elongational component at 45 degrees (we checked that these lines are not finite size effects by changing the box shape). Indeed, the tank-treading motion creates very little dissipation inside the vesicle. This is not itself a surprise since for a purely circular shape ($\tau=1$), the internal flow is purely rotational and therefore does not dissipate energy at all. At lower values of τ, the shape does no more permit a pure rotational flow inside the vesicle and dissipation occurs. From expression (9) we can expect the following dependence for the internal dissipation:

$$\dot{E}_{in} \propto \eta_{in} v_{tt}^2 (1-\tau)^{\alpha}, \tag{10}$$

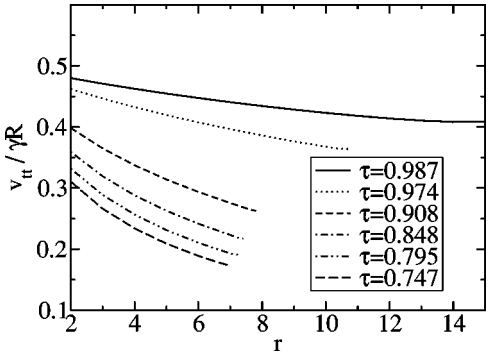

FIG. 8. Tank-treading velocity as a function of the viscosity ratio for various values of τ.

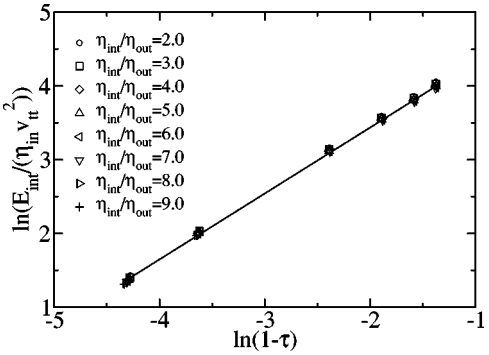

FIG. 9. Log-log plot of the internal dissipation rate.

where v_{tt} is the tank-treading velocity, which defines the velocity scale and α is an exponent which should be close to unity at low values of $1-\tau$. The variations of the internal dissipation are presented in Fig. 7, and we can observe the presence of a maximum. This maximum is in fact an artificial effect due to the normalization by η_{out}. The internal dissipation rate is in fact proportional to η_{in}, and the maximum results from a competition between growing values of r and a corresponding decrease of the tank-treading velocity (see Fig. 8). A normalization by η_{in} would have given monotonic decreasing curves (like v_{tt}). Amazingly, the tank-treading velocity seems to reach a minimum at the transition.

To check the validity of relation (10), in Fig. 9 we present a logarithmic plot of $\dot{E}_{in}/(\eta v_{tt}^2)$ as a function of $1-\tau$ for eight different values of the viscosity ratio, and we can see that they nicely superimpose on a master straight line of slope $\alpha=0.9$.

The external dissipation rate is presented in Fig. 10. First, as already mentioned, the external dissipation is larger than the dissipation inside the vesicle. Indeed the external dissipation is dominated by the shear itself, and is thus, strictly speaking, infinite. To analyze the contribution due to the vesicle we have subtracted the shear part and considered $E_{out}=\dot{E}_{out}-\eta_{out}\gamma^2 L^2$, L is the length of the resolution box. Even with this prescription, the contribution of the vesicle remains larger outside than inside (a factor of 10). A scaling law is, however, more difficult to obtain since dissipation outside the vesicle does not cancel when the tank-treading

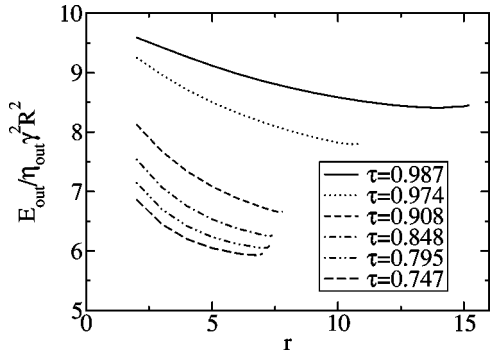

FIG. 10. External vesicular dissipation rate as a function of the viscosity ratio. The contribution of the external shear has been subtracted.

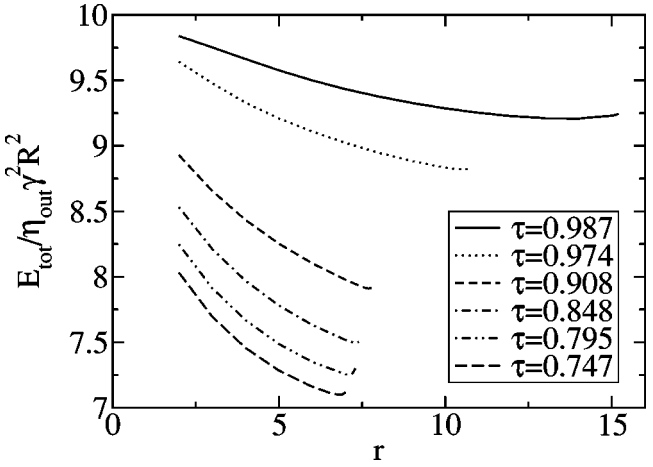

FIG. 11. Global dissipation rate as a function of the viscosity ratio.

velocity vanishes. We can observe that the external dissipation decreases when the vesicle becomes more elongated (decreasing values of τ) and when the viscosity ratio increases, in both cases the equilibrium angle θ decreases.

The total dissipation in the system is plotted in Fig. 11 and is very similar to the external dissipation presented in Fig. 10, which is the leading contribution. Amazingly, the global dissipation seems to exhibit a minimum close to the tumbling transition. But it is difficult to make conclusion, since numerical uncertainties are amplified close to the transition point.

Above the critical viscosity ratio no stationary angle exists, as predicted by Keller and Skalak, rather, a tumbling motion occurs according to the motion law (8). This equation is remarkably well satisfied, as shown in Fig. 12, even though the reduced surface $\tau=0.747$ corresponds to a region where the KS theory should become quantitatively insufficient (although qualitatively quite good).

This figure shows that the tumbling motion is not a regular rotation (the density of points, sampled at a fixed frequency, is not constant), especially close to the transition, rather, the tumbling motion is slow around $\theta=0$ and is fast for $\theta=\pi/2$. We can also see that the predicted KS value $A=-\gamma/2$ is well reproduced here. Superimposed to the tumbling, i.e. the rotation of the main axis, remains a tank-treading motion. Tank treading can be studied by computing

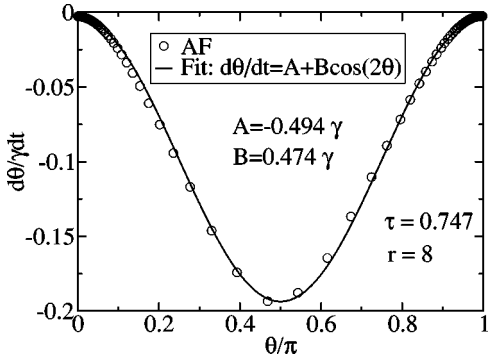

FIG. 12. Test of the dynamical equation for θ.

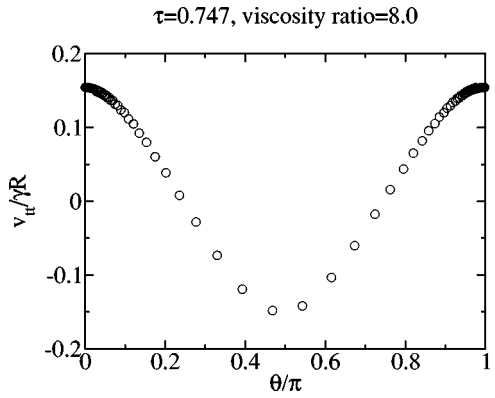

FIG. 13. Residual tank-treading velocity in the tumbling frame.

the velocity field along the membrane in the tumbling frame. A variation of the tank-treading velocity is presented in Fig. 13, where we observe the oscillatory behavior predicted by Keller and Skalak.

In this figure positive values of v_{tt} correspond to a clockwise tank treading while negative values to an anticlockwise rotation, which means opposite to the tumbling motion. Tank treading cancels for $\theta=\pi/4$ and $3\pi/4$. This oscillatory motion is well described in the paper by Keller and Skalak, so we will not enter into details here; we simply mention that this residual tank-treading velocity is five times smaller than in the pure tank-treading regime. Since the motion is now unsteady we expect transient effects to be important. The relaxation of the elastic constraints that applies on the membrane are not instantaneous either in nature or in simulations. A basic test is to analyze the variation of the tank-treading velocity along the contour of the vesicle. A perfectly inextensible membrane would correspond to a constant velocity along the contour. For our weakly extensible situation this is not indeed the case, and to quantify the variations of the tank-treading velocity we consider two extreme situations: $\theta\simeq 0$ (Fig. 14), which corresponds to a very slow tumbling motion (we are close to the tumbling transition) in which case the tension of the membrane is expected to be well equilibrated; and $\theta\simeq\pi/2$ (Fig. 15), which is the worse situation for the membrane since the tumbling motion is very fast at that point of the trajectory and the tension of the membrane has little time to relax.

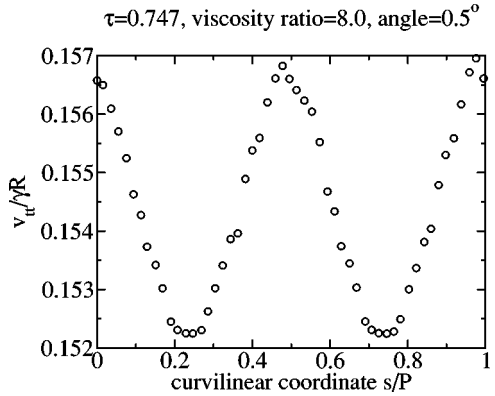

FIG. 14. Tank treading velocity along the membrane for $\theta=0.5$ degrees.

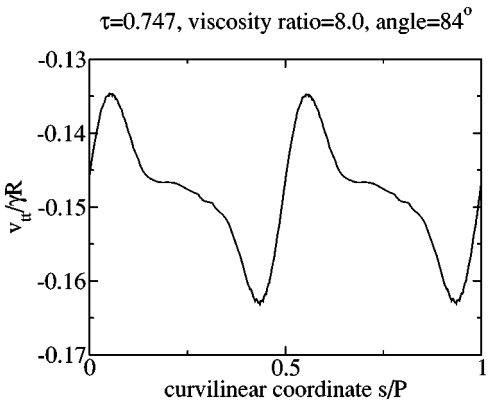

FIG. 15. Tank-treading velocity along the membrane for $\theta=84$ degrees.

It is then not a surprise if the variation of the tank-treading velocity along the contour is much more important in the second case (20% in amplitude) than in the first one (3%). The variation was only 1% in the steady tank-treading regime (see Fig. 16).

As for the tank-treading case, dissipation can be analyzed inside and outside the vesicle during its rotation. In Fig. 17 we show the variations of the internal dissipation rate as a function of the instantaneous orientation of the vesicle. Not surprisingly, dissipation is maximized when the modulus of the tank-treading velocity reaches its maximum, i.e., when $\theta=0$ and $\pi/2$. Figure 18 shows the corresponding variation of the external dissipation, and we can see that internal and external dissipation vary in opposite phase.

Although the variation of the internal dissipation is directly related to tank-treading, the external dissipation is more complicated since both tank-treading, tumbling and excluded volume effects play a role. The complementarity of the internal and external dissipation is then not complete which is illustrated by the variation of the global dissipation (see Fig. 19). As in the tank-treading regime, the internal dissipation is only a fraction of the total dissipation due to the vesicle (10%).

IV. CONFINEMENT EFFECTS

In order to tend towards a more realistic description of the tank treading-tumbling transition, it appears necessary to

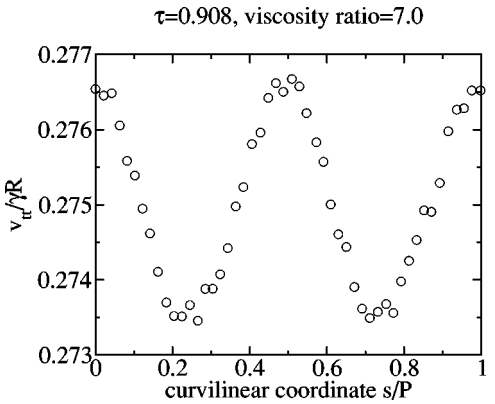

FIG. 16. Variation of the tank-treading velocity along the membrane in the tank-treading regime.

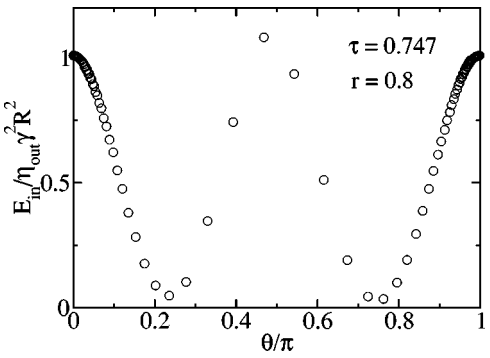

FIG. 17. Internal dissipation rate as a function of θ.

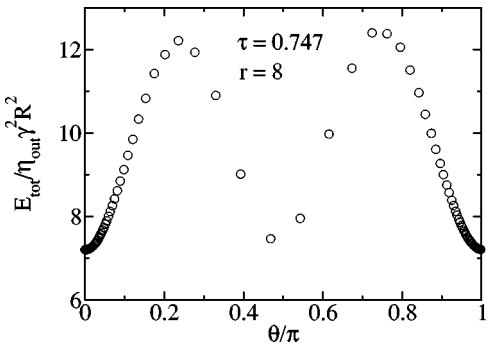

FIG. 19. Global dissipation rate as a function of θ.

modify slightly the system. We considered the highly idealized case of an isolated vesicle submitted to a constant shear flow, but in practice we have to take into account the confinement effects, simply because this corresponds to the experimental situation. The rheology of blood in capillaries, for example, exhibits features directly related to confinement: the apparent viscosity depends of the vessel diameter; this is the so-called Farhaeus-Lindquist effect. We will, however, not consider here the geometry of a capillary tube, since the flow in such situations is quadratic (Poiseuille flow). This type of flow is known to induce lift forces on vesicles or red blood cells which tend to group the cells at the center of the tube. On the axis of the tube however, shear cancels. This geometry is then not very appropriate to investigate shear effects. Rather, we will confine the vesicle between two plates, each of them moving in opposite directions. To eliminate drifts due to the lift force [19] the vesicle is placed at the center of the cell. Since the plates move in opposite directions, a shear remains at that point controlled by the relative velocity of the plates. This geometry can easily be incorporated in the AF method: we just have to introduce a no-slip boundary condition on the plates located at the top and the bottom of the resolution box. The top and bottom boundary conditions now correspond to a cancellation of the flow induced by the vesicle (the total velocity field minus the imposed shear flow), whereas we previously considered periodic boundary conditions for this component of the flow.

In Fig. 20 we plot the critical viscosity ratio as a function of the confinement R/L, where L is the distance between the shearing plates. We can observe that the critical viscosity ratio increases rapidly when the distance between the plates is reduced. It reaches even twice the bulk value when the distance between the plates is of the order of seven times the effective radius R, which is not that a strong confinement. The extrapolated bulk value is obtained to be $r_c=5.5$ which is very close to the value $r_c=5.4$ obtained with periodic boundary conditions (but no rigid walls at the boundaries) as shown in Fig. 26. The transition curve is presented in Fig. 21, obtained as explained above. The lower curve corresponds to an isolated vesicle, and the upper one to a vesicle between two plates, with a confinement of $R/L=0.13$. As expected, due to the geometrical constraints, the critical viscosity ratio is sensitively increased in the case of the nonvanishing confinement. It is not a surprise in itself because of the increase of the dissipation between the vesicle and the plates. The energy needed for the vesicle to tumble is in a sort dissipated.

Of course, a further quantitative analysis of the dissipation is required in this geometry, but a strong dependence of the rheology of such a binary system under confinement can be expected at this level.

V. DISCUSSION

The KS theory seems to provide an accurate description of the physics involved in the dynamics of vesicles in a shear flow. We checked that the theory is qualitatively excellent, and gives quite good quantitative predictions for vesicles in two dimensions. A 3D numerical calculation (with no viscosity contrast) [20] regarding the pure tank-treading motion

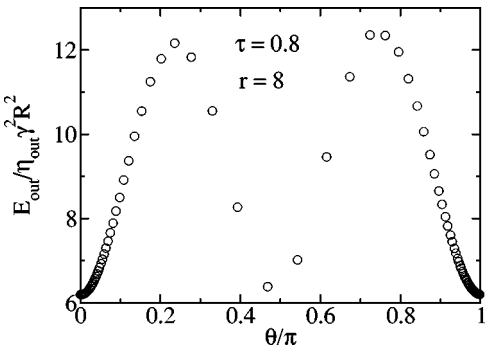

FIG. 18. External dissipation rate as a function of θ. The shear contribution has been subtracted.

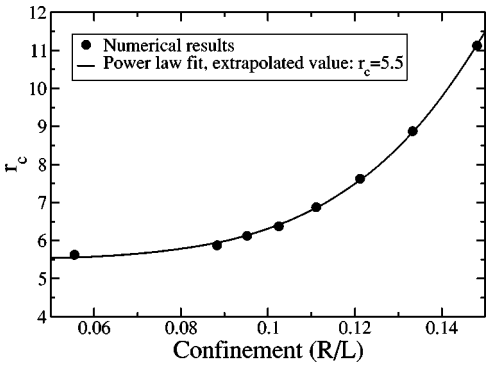

FIG. 20. Variation of r_c as a function of the confinement. Here $\tau=0.8$.

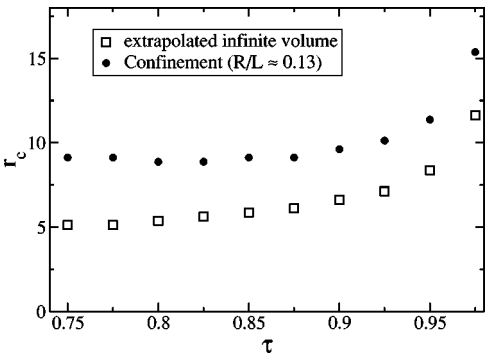

FIG. 21. Here we plot the tank-treading to tumbling transition curve for a confinement $R/L=0.13$ and the extrapolated bulk transition curve.

arrived to the same conclusion for this motion. This result is not fully intuitive, since the theory does not incorporate the physics of the membrane itself (the shape is assumed to be ellipsoidal). We could check numerically that in the free boundary problem the curvature deformability C_κ of the vesicle does not play a key role, at least in the regime $C_\kappa < 1$ corresponding to a weak deformability. Indeed, the main physical ingredients in this problem seem to be the geometrical constraints of fixed perimeter and area (surface and volume in three dimensions), captured by the KS theory. Interestingly, these properties are common to vesicles and red blood cells, which may explain the observed similarities between red blood cells and vesicles in a shear flow. But the comparison is not complete, and several features of the red blood cell motions are not accounted for by a simple vesicle model. As an example, the shear rate only defines a time scale in the KS theory; it simply appears as a prefactor in dynamical quantities and can therefore be eliminated by rescaling time. As a consequence, the transition threshold does not depend on the shear rate, which is not fully the case for red blood cells. We can then conclude that other time scales should play a role in the dynamics of red blood cells, and that the dependence of the transition in the shear rate should come from a competition between the forced time scale γ and internal time scales of the cell. These internal time scales also exist for vesicles; $t_{shape}=\eta R^3/\kappa$ is the relaxation time of the shape at fixed perimeter (surface in three dimensions), and C_κ expresses precisely the competition between the deformation imposed to the vesicle by the shear flow and the relaxation of the shape due to the curvature energy. However, we have seen that the dependence in C_κ is very weak in the low deformability regime. The situation may change in the large deformability regime, but we have not yet investigated this regime. A second internal time scale appears in our formulation due to our prescription for the Lagrange's parameter field: the membrane is not strictly inextensible. Extensibility introduces a new relaxation time scale, associated to the perimeter (or the surface in three dimensions) which we chose very small compared to t_{shape} and γ^{-1} (of the order of 10^{-3}) so that the constraint is almost instantaneously satisfied. We could, however, consider more deformable entities and expect a shear dependence of the results in this case. At least another time scale enters into play for red blood cells since the membrane has a shear modulus, which again defines a relaxation scale. Account of these various relaxation scales lead to quite complex behaviors, as illustrated in [14]. Reducing the complexity motivated our simplistic approach where time scales are included progressively. A study of extensible membranes is currently in progress. Introduction of the full complexity does not affect the overall picture of the tank-treading to tumbling transition. The transition is simply more progressive, oscillations have indeed been observed in its neighborhood that rends the experimental or numerical analysis more difficult. The vesicle model presents, on the contrary, a sharp transition, and thus confinement effects, or collective effects if several vesicles interact can be interpreted more easily. The transition itself has been investigated in this article on the basis of a dissipation analysis. This analysis reveals that most of the dissipation occurs outside the vesicle, the flow inside the vesicle rotates in quasi-solid manner and does not generate a significant shear. This point is important since it indicates that a non-linear behavior of the encapsulated fluid will probably not affect too much the results. Viscoelasticity will, on the contrary, define new time scales which will compete with all the other times scales of the system, as previously discussed. We thus expect viscoelastic behaviors of the encapsulated fluid to be more visible than non-linearities (the study is, however, still to be done). On the same ground, a precise description of the flow outside the vesicle seems to be more important than the description inside, and this may be the reason why the KS theory works so well: it is based on Jeffery's analytic solution for rigid ellipsoids outside the particle. The tank-treading motion being introduced in an approximate way, it does not strictly satisfy the local inextensibility of the membrane, which affects the flow inside (it is the main component) much more than outside (it is only part of the flow). The tumbling motion is simply a global rotation. This dissipation analysis also shows several intriguing features: The total dissipation decreases as we approach the transition where it seems to be minimal (the derivative cancels). In the tumbling regime dissipation oscillates, the internal and external dissipation are out of phase, which expresses an exchange between the tumbling motion (large dissipation outside, low dissipation inside) and the tank-treading motion (low dissipation outside, large dissipation inside). We could then expect the oscillations to compensate, but this is not the case since the amplitude of the external oscillations is much larger than the internal ones. The internal dissipation is indeed directly related to the residual tank-treading motion in the tumbling regime, and is therefore very small (v_{tt} is five time smaller in the tumbling regime than in the tank-treading regime for the parameters we have considered). A dissipation analysis would be also interesting in confined situations where we observe a strong effect of the confinement on the transition location: confinement favors the tank-treading regime. The rheological consequences have not yet been investigated, but this is certainly a problem to consider.

VI. CONCLUSION

We have presented a numerical study of the tank-treading to tumbling transition in vesicular systems, based on the Hel-

frich formulation, and compared our results to the KS theory. We have first compared the newly proposed AF method to the boundary integral formulation, and have shown that the AF formulation can provide quantitative results when finite size effects and the sharp interface limit are considered. A comparison of our results with the KS theory shows that although slight quantitative discrepancies exist, the KS theory represents a very good framework for the investigation of the dynamics of a single vesicle in a shear flow. In the low deformability regime $C_\kappa < 1$ the boundary integral formulation shows that indeed the results are independent of C_κ which is a basic assumption in the KS theory. An analysis of the dissipation in the system shows that the main contribution (once the shear contribution has been removed) comes from the external flow; the internal fluid rotation represents only 10% of the dissipation. In the tumbling regime we observe oscillations of the dissipation, with an opposite phase for the internal and external dissipation, indicating an exchange between the tumbling motion and the residual tank treading. Finally, we have analyzed the confinement effects on the transition and shown that the critical transition line is strongly shifted by the confinement (even when the box size is five times larger than the vesicle). We believe that this effect should have strong consequences on the rheological properties of the medium.

There are several features which have not been discussed here, since our first focus was to make the presentation as simple as possible. First, we have treated the two monolayers as forming a single entity; that is, we did not account for a relative sliding between the two monolayers [21]. If the dissipation associated with the relative motion becomes comparable to that in the bulk, we expect this to affect the tumbling transition. Most important is that we have confined our study to 2D vesicles, and this assumption must be relaxed in the future if one whishes to have a more quantitative comparison with experiments. Several other ingredients must then be incorporated such as the spontaneous curvature and the area difference between the two monolayers, two ingredients that have proven to be essential in describing the equilibrium shapes of vesicles. We have developed an AF approach in three dimensions, and it turns out that speeding up the computation efficiency is imperative before performing a systematic quantitative study. This question is under consideration.

ACKNOWLEDGMENT

This work received a support from the ''Institut de Physique de la Matière Condensée'' (IPMC, Grenoble, France).

APPENDIX A: BOUNDARY INTEGRAL METHOD

The boundary integral method is the traditional technique used to solve classical hydrodynamical problems in the Stokes limit. The method is based on the resolution of the Stokes equations (2) using the Green function's formalism. Since we consider a two-fluid problem, the internal fluid with viscosity η_{in} and the external fluid with viscosity η_{out}, it is interesting to separate the integration domain into two subspaces: Ω_{in}, the internal medium, and Ω_{out}, the external fluid. The boundary between these two domains will correspond to the membrane forming the vesicle. Let us first consider an homogeneous fluid with generic viscosity η flowing in a generic domain Ω. We assume moreover that the fluid is subjected to a force field $\mathbf{f}(\mathbf{r})$ defined in Ω. In the Stokes limit, the flow is obtained by solving the Stokes equation for incompressible Newtonian fluids:

$$\eta \Delta \mathbf{v} - \boldsymbol{\nabla} p + \mathbf{f} = \mathbf{0}, \qquad \boldsymbol{\nabla} \cdot \mathbf{v} = \mathbf{0}. \tag{A1}$$

These equations have to be supplemented by appropriate boundary conditions at the edge of the integration domain Ω. The derivation of both the integral equations together with the Green's functions have been discussed at length in Ref. [22], so we shall just briefly recall the main steps, and emphasize on how a viscosity contrast must be incorporated. If Ω is the full space, and boundary conditions at infinity are $\mathbf{v}=0$ and no surface force apply at infinity, we can expect linear relations between the velocity field $\mathbf{v}$ (the pressure field p) and the force field $\mathbf{f}$ of the forms

$$\eta \mathbf{v}_0(\mathbf{r}) = \int_\Omega \overline{G}(\mathbf{r}-\mathbf{r}')\mathbf{f}(\mathbf{r}')d\mathbf{r}',$$

$$p_0 = \int_\Omega \mathbf{q}(\mathbf{r}-\mathbf{r}')\cdot\mathbf{f}(\mathbf{r}')d\mathbf{r}'.$$

Insertion of these expressions into the Stokes equation (A1) leads to the equation for the Green tensor $\overline{G}$ and the Green vector $\mathbf{q}$:

$$\partial_{kk} G_{il} - \partial_i q_l = -\delta(\mathbf{r}-\mathbf{r}')\delta_{il}, \qquad \partial_k G_{ik} = 0,$$

where indices i, l, and k stand for the components of $\overline{G}$ and $\mathbf{q}$ along the x, y, and z axes; ∂_i is a derivation along the i axis, and a summation over repeated indices (Einstein convention) is assumed. When surface forces apply at the edge $\partial\Omega$ of the integration domain Ω or the velocity field does not cancel, extra contributions appear, and the generic expression for the velocity field is

$$\eta\delta(\mathbf{r},\Omega)\mathbf{v}(\mathbf{r}) = \int_\Omega \overline{G}(\mathbf{r}-\mathbf{r}')\mathbf{f}(\mathbf{r}')d\mathbf{r}' + \int_{\partial\Omega} \overline{G}(\mathbf{r}-\mathbf{r}')\mathbf{f_s}(\mathbf{r}')d\mathbf{r}' + \eta\int_{\partial\Omega} \mathbf{v}(\mathbf{r}')\cdot\overline{K}(\mathbf{r}-\mathbf{r}')\cdot\hat{\mathbf{n}}(\mathbf{r}')d\mathbf{r}', \tag{A2}$$

where $\mathbf{f_s}$ are the surface forces at the boundary, and $\hat{\mathbf{n}}$ is the normal vector at the boundary pointing outside Ω. $\delta(\mathbf{r},\Omega)$ is unity when $\mathbf{r}$ is located inside Ω, and half when $\mathbf{r}$ is at the boundary and zero outside. $\overline{K}$ is a third order tensor. The two

first contributions account for the external volume and surface forces applying on the fluid located in Ω while the last term accounts for a non-vanishing velocity field at the border. Expressions for $\overline{G}$ and $\overline{K}$ in three dimensions are [22]

$$\overline{K}_{ijk}^{3D}=\frac{3}{4\pi}\frac{x_i x_j x_k}{x^5},$$

$$\overline{G}_{ij}^{3D}=\frac{1}{8\pi}\left(\frac{\delta_{ij}}{x}+\frac{x_i x_j}{\dot{x}^3}\right).$$

Here $\mathbf{x}$ stands for $\mathbf{r}-\mathbf{r}'$ and x is the modulus of $\mathbf{x}$. The 2D expression for these tensors can be obtained by integration along the z axis:

$$\overline{K}_{ijk}^{2D}=\frac{1}{\pi}\frac{\dot{x}_i x_j x_k}{x^4},$$

$$\overline{G}_{ij}^{2D}=\frac{1}{4\pi}\left(-\delta_{ij}\log(x)+\frac{x_i x_j}{x^2}\right).$$

Care must be taken [23] while integrating $\overline{G}$ since a logarithmic divergence occurs; a cutoff in the z direction can be introduced which does not play any role when the integral of the external forces applied on the system vanishes (the situation here).

The generic equation (A2) can now be applied to the external and internal media forming the vesicle, Ω_{out} and Ω_{in}. In the absence of external forces, the velocity field at the membrane can be written from Eq. (A2):

$$\begin{aligned}\frac{\eta_{in}}{2}\mathbf{v}_{mem}(\mathbf{r})&=\int_{mem}\overline{G}(\mathbf{r}-\mathbf{r}')\mathbf{f}_{\mathbf{s}}^{in}(\mathbf{r}')d\mathbf{r}'\\&\quad+\eta_{in}\int_{mem}\mathbf{v}(\mathbf{r}')\cdot\overline{K}(\mathbf{r}-\mathbf{r}')\cdot\hat{\mathbf{n}}^{in}(\mathbf{r}')d\mathbf{r}'\\ \frac{\eta_{out}}{2}\mathbf{v}_{mem}(\mathbf{r})&=\int_{mem}\overline{G}(\mathbf{r}-\mathbf{r}')\mathbf{f}_{\mathbf{s}}^{out}(\mathbf{r}')d\mathbf{r}'\\&\quad+\eta_{out}\int_{mem}\mathbf{v}(\mathbf{r}')\cdot\overline{K}(\mathbf{r}-\mathbf{r}')\cdot\hat{\mathbf{n}}^{out}(\mathbf{r}')d\mathbf{r}'\\&\quad+\eta_{out}\int_{infinity}\mathbf{v}(\mathbf{r}')\cdot\overline{K}(\mathbf{r}-\mathbf{r}')\cdot\hat{\mathbf{n}}^{out}(\mathbf{r}')d\mathbf{r}',\end{aligned}\tag{A3}$$

where "*mem*" denotes the membrane and "*infinity*" the contour at infinity, $\mathbf{f}_{\mathbf{s}}^{in}$ and $\mathbf{f}_{\mathbf{s}}^{out}$ are the surface forces applied respectively to the internal and external fluid at the membrane, this force is due to the membrane, and therefore $\mathbf{f}_{\mathbf{s}}^{in}+\mathbf{f}_{\mathbf{s}}^{out}=\mathbf{f}_{mem}$. The last term in the second equation of Eqs. (A3) accounts for the externally applied flow (shear in the present situation). Summation of these two expressions leads to

$$\begin{aligned}&\frac{\eta_{in}+\eta_{out}}{2}\mathbf{v}_{mem}(\mathbf{r})\\&\quad=\int_{mem}\overline{G}(\mathbf{r}-\mathbf{r}')\mathbf{f}_{mem}(\mathbf{r}')d\mathbf{r}'+(\eta_{in}-\eta_{out})\\&\qquad\times\int_{mem}\mathbf{v}(\mathbf{r}')\cdot\overline{K}(\mathbf{r}-\mathbf{r}')\cdot\hat{\mathbf{n}}(\mathbf{r}')d\mathbf{r}'b+\eta_{out}\mathbf{v}_{shear},\end{aligned}\tag{A4}$$

where $\hat{\mathbf{n}}$ is now the normal vector pointing outside the vesicle.

The membrane force $\mathbf{f}_{mem}$ is deduced from the Helfrich free energy

$$E_H=\int_{memb}\left\{\frac{\kappa}{2}c^2+\zeta(s)\right\}ds.$$

c is the local curvature of the shape and the factor ζ is the Lagrangian parameter which ensures a constant perimeter for the vesicle. Note that both the inner and the outer fluids are supposed to be incompressible. A second Lagrangian parameter to ensure a constant surface for the vesicle is thus useless in our case. The membrane force is derived from the free energy by the equation

$$\mathbf{f}_{mem}=-\frac{\delta E_H}{\delta\mathbf{r}}.$$

In two dimensions [19],

$$\mathbf{f}_{mem}=-\kappa\left(\frac{d^2c}{ds^2}+\frac{c^3}{2}\hat{\mathbf{n}}\right)+\frac{d\zeta}{ds}\hat{\mathbf{t}}+c\zeta\hat{\mathbf{n}}\tag{A5}$$

where $\hat{\mathbf{t}}$ is the tangent vector at the membrane, $(\hat{\mathbf{t}},\hat{\mathbf{n}})$ form a direct ortho-normal basis, and c is defined by $d\hat{\mathbf{t}}/ds=+c\hat{\mathbf{n}}$, s is the curvilinear coordinate. The first two terms are curvature forces. The third term describes the adjustable force necessary to ensure a constant perimeter, and can be interpreted as a Marangoni effect. The fourth term is the well-known Laplace force. This force stemes from the pressure difference linked to curvature effects on both sides of the membrane.

The numerical procedure is simple: from the shape of the vesicle we can compute the membrane force $\mathbf{f}_{mem}$. The knowledge of $\mathbf{f}_{mem}$ allows us to get the expression of the velocity field at the membrane interface thanks to the integral formulation (A4) and thus to predict its motion. The basic numerical strategy was described in Ref. [23].

APPENDIX B: ADVECTED-FIELD APPROACH

1. Definitions

Alternatively, Eqs. (6) can be modified to derive a more flexible scheme which applies to various physical situations (boundary conditions or complex non-Newtonian fluids). The idea is to replace the so-called "sharp interface" problem presented above by a smooth interface [17]. The vesicle is now described by an advected-field ϕ which goes

smoothly from -1 to $+1$ while crossing the membrane. -1 will for example represent the internal part of the vesicle and $+1$ the external fluid, the membrane being located at the zeros of the AF. Obviously we must recover the ''sharp interface'' description when the width ϵ of the ''smooth interface'' goes to zero. This limit is called the ''sharp interface limit'' and will be presented in a forthcoming publication. A simple way to produce a field going from -1 to $+1$ with a typical interfacial size ϵ is to consider the following functional:

$$E_{intrinsic}[\phi]=\int\int dxdy\left\{\frac{1}{4}(1-\phi^2)^2+\frac{\epsilon^2}{2}(\nabla\phi)^2\right\}. \tag{B1}$$

This functional corresponds to the simplest Landau-Ginzburg description of a binary interface, the square-gradient theory. Minimization of this functional in the special case of a flat interface leads to the following interfacial profile:

$$\phi(r)=\tanh(r/\epsilon\sqrt{2}), \tag{B2}$$

where r is the coordinate in the normal direction, with the convention that $r=0$ at the interface. We have explicitly used the boundary conditions $\phi(\pm\infty)=\pm 1$ and $\phi'(\pm\infty)=0$. When the interface is curved, however, the Laplace force contained in Eq. (B1) induces a curvature dependence of the shape. Elimination of this force is thus necessary to keep the hyperbolic tangent shape (B2), and to suppress spurious relaxations, as will be discussed later.

To obtain the full energy functional of the vesicle within the AF approach, we have to generalize what we called the configurational energy (E) in Appendix A. To this end, we need to introduce a coordinate perpendicular to the membrane (r) and rewrite the integrals along the membrane in the following way:

$$\int ds\rightarrow\int ds\int dr\,\delta^{shape}(r),$$

where $\delta^{shape}(r)$ is the ''shape function'' of the membrane which should reduce to a Dirac distribution centered on the membrane in the sharp interface limit. From its definition $\delta^{shape}(r)$ must satisfy the normalization condition $\int dr\,\delta^{shape}(r)=1$. A convenient choice for this function is, in Cartesian coordinates,

$$\delta^{shape}(\mathbf{r})=\frac{|\nabla\phi|}{2}, \tag{B3}$$

which satisfies the normalization condition since the advected field goes from -1 to 1 while crossing the membrane. Here, $\mathbf{r}$ denotes the current position in Cartesian coordinates. Expression (4) of the configurational energy can then be easily extended as follows:

$$E_{config}=\frac{\kappa}{2}\int\int dxdy c^2\frac{|\nabla\phi|}{2}+\int\int dxdy\zeta\frac{|\nabla\phi|}{2}. \tag{B4}$$

The curvature field c can easily be expressed in terms of the AF if we define the normal vector field $\hat{\mathbf{n}}$ and the tangential vector field $\hat{\mathbf{t}}$ as

$$\hat{\mathbf{n}}=\frac{\nabla\phi}{|\nabla\phi|},$$

$$\hat{\mathbf{t}}=\hat{\mathbf{n}}\times\hat{\mathbf{z}}. \tag{B5}$$

Here $\hat{\mathbf{z}}$ is the unit vector normal to the 2D plane. This definition corresponds to the choice

$$\frac{d\hat{\mathbf{t}}}{ds}=+c\hat{\mathbf{n}} \tag{B6}$$

in curvilinear coordinates. One can easily check that the curvature field satisfies

$$c=-\nabla\cdot\hat{\mathbf{n}}. \tag{B7}$$

ζ is a more complex field which cannot be expressed as a simple functional of ϕ (it is history dependent, as we will see).

2. Expression of the force

To obtain an explicit expression for the external force $\mathbf{f}_{ext}$ it is necessary to differentiate the configurational energy E_{config} with respect to the local position of the membrane. A local displacement of the membrane by a vector $\delta\mathbf{R}$ corresponds to the transformation $\phi(\mathbf{r})\rightarrow\phi(\mathbf{r}-\delta\mathbf{R})$ [e.g., $\zeta(\mathbf{r})\rightarrow\zeta(\mathbf{r}-\delta\mathbf{R})$]. As a result,

$$\frac{\delta\phi}{\delta\mathbf{R}}=-\nabla\phi=-|\nabla\phi|\hat{\mathbf{n}}=-2\,\delta^{shape}(\mathbf{r})\hat{\mathbf{n}},$$

$$\frac{\delta\zeta}{\delta\mathbf{R}}=-\nabla\zeta. \tag{B8}$$

From these expressions we can easily see that all contributions to the total energy E having a functional dependence in ϕ will give rise to normal forces, as a result, the only contribution that leading to a tangential force is the ζ term. Since the derivation of the force is a bit tedious (see Appendix D) we simply write down the final expression here:

$$\mathbf{F}_{config}=\left[-\kappa\left\{\frac{c^3}{2}+\hat{\mathbf{t}}\cdot\nabla(\hat{\mathbf{t}}\cdot\nabla c)\right\}\hat{\mathbf{n}}+\zeta c\hat{\mathbf{n}}+\hat{\mathbf{t}}\cdot\nabla\zeta\hat{\mathbf{t}}\right]\delta^{shape}(\mathbf{r}), \tag{B9}$$

which is to be compared to its analog (A5) in the sharp interface limit [19], with prescription (B6) for the curvature:

$$\mathbf{F}_{config}=\mathbf{f}_{mem}=-\kappa\left\{\frac{c^3}{2}+\frac{d^2c}{ds^2}\right\}\hat{\mathbf{n}}+\zeta c\hat{\mathbf{n}}+\frac{d\zeta}{ds}\hat{t}, \tag{B10}$$

where s is the curvilinear coordinate. From these two expressions we can note that $\hat{t}\cdot\nabla$ is the natural extension of d/ds.

3. Final equations

Velocity field: Expression (B9) allows to calculate explicitly the local force $\mathbf{f}_{ext}$ acting on the velocity field for a given configuration of the AF $\phi(\mathbf{r})$. The Stokes equation can be solved using a relaxation scheme:

$$\epsilon_v \frac{\partial \mathbf{v}}{\partial t} = \nabla \cdot [\,\eta(\nabla \mathbf{v} + \nabla \mathbf{v}^T)\,] - \nabla P + \mathbf{f}_{ext}, \qquad \text{(B11)}$$

where ϵ_v is a density scale which is related to the relaxation time (and thus defines an effective Reynolds number), and $\mathbf{f}_{ext} \equiv \mathbf{F}_{config}$ as given by expression (B9). The pressure field must be adjusted to ensure incompressibility:

$$\nabla \cdot \mathbf{v} = 0.$$

When a viscosity contrast exists between the fluid enclosed into the vesicle and the external fluid, η is position dependent. A simple prescription for η is to set $\eta = \eta_{out}(1+\phi)/2 + \eta_{in}(1-\phi)/2$ which guarantee a continuous variation of viscosity while crossing the membrane. We used this prescription here.

Advected field: The dynamical equation for the AF can be derived from the condition $\mathbf{v}_{mem} = \mathbf{v}$ which specifies that the membrane is simply advected by the flow. Pure advection is unfortunately not numerically stable with ordinary numerical schemes, and it does not guarantee that the final shape of the AF minimizes the energy functional (B1). To cure this problem, we can write the following dynamical equation:

$$\frac{\partial \phi}{\partial t} = -\mathbf{v} \cdot \nabla \phi + \epsilon_\phi \left(-\frac{\delta E_{intrinsic}}{\delta \phi} + c\epsilon^2 |\nabla \phi| \right), \qquad \text{(B12)}$$

where we recognize the advection contribution $-\mathbf{v} \cdot \nabla \phi$ and the restoring force $-\delta E_{intrinsic}/\delta\phi$. Note the presence of an additional term, $c\epsilon^2|\nabla\phi|$, as suggested by Folch *et al.* [24], that plays a very important role in the AF method. To understand the role of this counter-term, it is interesting to write the dynamical equation in a more explicit way, using the prescription (B1) for the functional:

$$\frac{\partial \phi}{\partial t} = -\mathbf{v} \cdot \nabla \phi + \epsilon_\phi (\phi(1-\phi^2) + \epsilon^2(\Delta\phi + c|\nabla\phi|)).$$

We show in Appendix E that in the sharp interface limit ($\epsilon \to 0$), using the dimensionless rescaled variable $r^* = r/\epsilon$, the combination $\Delta\phi + c|\nabla\phi|$ simply reduces to $\partial^2\phi/\partial r^{*2} + \mathcal{O}(\epsilon^2)$. The steady AF profile across the interface reduces then, up to order ϵ^2, to the profile of the *planar* interface (B2), and is thus not sensitive to the local curvature. The physical implication is that the lateral relaxation of the global shape induced by the Laplace force due to the surface tension of the Landau-Ginzburg theory has been suppressed [the counterterm corresponds precisely to the opposite of the Laplace force, which can be checked by integrating this counter term across the interface, with expression (B3) for the shape function]. An important consequence, justifying the name of the method, is that the AF is quasipassive: it is simply transported by the flow, whereas in the absence of the counterterm, the vesicle would simply disappear to minimize $E_{intrinsic}$. Since terms of order ϵ^2 remain, drifts can be observed after a while, but since in most numerical implementations the grid spacing h is of the order of ϵ, and the usual discretization of the differential operators is of order h^2, it is in practice useless to go beyond ϵ. The key point is then to adjust the value of ϵ_ϕ such that the drifts remain negligible while the numerical scheme remains stable. In practice, ϵ_ϕ is of the order of unity. Although the counterterm cancels the first order in ϵ in the AF equation, corrections of order ϵ are still present in the velocity equation, and thus linear dependences of the results in ϵ can be expected in general. But these corrections only affect the results in a quantitative way as we will see below.

Lagrange's parameter field: The last equation concerns the Lagrange's parameter field ζ that appears in the force associated to the constraint of fixed local length of the membrane [see Eq. (B10)]. Unfortunately the functional relation between the perimeter and ζ is not known explicitly. We will then use a prescription based on a physical interpretation of ζ, namely that this field corresponds to a local tension of the membrane. In a linear response theory we can assume that this tension is proportional to the local extension of the membrane. From this interpretation, we postulate a phenomenological equation for ζ:

$$\frac{d\zeta}{dt} = -\mathbf{v} \cdot \nabla \zeta + T\hat{\mathbf{t}} \cdot (\hat{\mathbf{t}} \cdot \nabla)\mathbf{v}, \qquad \text{(B13)}$$

where T is a ''tension'' constant (energy per unit surface) and $\hat{\mathbf{t}} \cdot (\hat{\mathbf{t}} \cdot \nabla)\mathbf{v}$ simply represents $\hat{\mathbf{t}} \cdot \partial \mathbf{v}/\partial s$ in the sharp interface limit (s is then the curvilinear coordinate) which is nothing but the local extension rate of the membrane. With this prescription, ζ is proportional to the local extension of the membrane.

4. Numerical procedure and parameters

Both the advected field $\phi(\mathbf{r})$, the velocity field $\mathbf{v}(\mathbf{r})$ and the tension field $\zeta(\mathbf{r})$ are discretized on a square lattice of size $N_x \times N_y$ where N_x and N_y are taken of the order of 300, and the differential operators are discretized on this lattice using algorithms of order two cylindrically symmetric. Rotational symmetry is very important in this problem, and care has been taken to ensure it. Tests with the more symmetric hexagonal lattice have been performed providing the same results. From an initial configuration of $\phi(\mathbf{r})$, $\mathbf{v}(\mathbf{r})$, and $\zeta(\mathbf{r})$ it is possible to compute their time evolution by integration of the equations presented in the previous section using a fourth order Runge-Kutta solver. Periodic boundary conditions have been used at the border of the simulation box for $\phi(\mathbf{r})$, $\zeta(\mathbf{r})$ and the velocity field induced by the vesicle (i.e., the actual velocity field minus the imposed external field). These periodic conditions on the relevant fields allowed for implicit algorithms in Fourier space, of special interest for solving the Stokes equation combined with the incompressibility constraint.

We have chosen the following system of units: the unit length is $R = \sqrt{S/\pi}$ where S is the surface of the vesicle, R is

then the typical radius of the vesicle which is of the order of $R \simeq 10\ \mu$m; the time unit is defined as the typical time for a vesicle to relax to its equilibrium shape $t_{shape} = \eta_{out} R^3/\kappa$; the mass unit is fixed by setting $\epsilon_v = 1$. The physical dimensionless control parameters are as follows.

$C_\kappa = \eta_{out}\gamma R^3/\kappa = \gamma t_{shape}$, the "curvature" number controlling the curvature deformability of the vesicle in the external flow. A large value of C_κ corresponds to a large deformation. In practice we set $C_\kappa = 0.5$, which corresponds to an intermediate regime.

$C_T = \eta_{out}\gamma R/T$, the "tension" number that controls the perimeter variation due the externalflow. A large value of C_T means a large extensibility of the membrane. Here we set C_T to 10^{-3} on the contrary, to ensure the constraint of fixed perimeter.

$\mathrm{Su} = \mathrm{Rc}/C_\kappa = \epsilon_v \kappa/\eta_{out}^2 R$, the Suratman number, which represents the Reynolds number Re estimated using t_{shape} as the typical time scale. This number is fixed to 10^{-2} in practice, since we work in the Stokes regime. Smaller values have been tested, slowing down the computation speed without affecting the results.

$r = \eta_{in}/\eta_{out}$, the viscosity contrast typically between 1 and 10 here.

$\tau = 4\pi S/P^2$, the swelling ratio in two dimensions (S is the internal area and P the perimeter), between 0.7 and 1.

The technical parameters associated to the AF equations or appearing in the numerical scheme are

ϵ	the interfacial width of typical value $0.035R$.
h	the lattice spacing $dx = dy = h = 0.03R$.
N_x, N_y	the number of grid points in a direction varies from 200 to 500.
dt	the time step is of the order of $10^{-3} t_{shape}$.
$t_\phi = 1/\epsilon_\phi$	the AF relaxation time is of the order of $0.2\ t_{shape}$.

APPENDIX C: TEST OF THE METHODS

1. Equilibrium shapes

When no external force is applied to a vesicle its shape relaxes to minimize the curvature energy with the constraint of a fixed perimeter P and a surface S. These equilibrium shapes have been thoroughly investigated in two or three dimensions by several authors, and can be obtained in the sharp interface description by a direct integration of the minimization equation using a shooting method. In Fig. 22 we compare the results obtained with the advected field method to the sharp interface description. In this figure circles correspond to the isocontour $\phi = 0$ of the advected field, and the solid line to the sharp interface data. We can see that these two methods are in fairly good agreement, whatever the value of the reduced surface $\tau = 4\pi S/P^2$. In Fig. 22 the perimeter has been arbitrarily fixed to $P = 2\pi$.

Since the KS theory assumes a fixed ellipsoidal shape for the vesicle, it is interesting to compare the actual equilibrium shapes to ellipsis. Such a comparison is presented in Fig. 23.

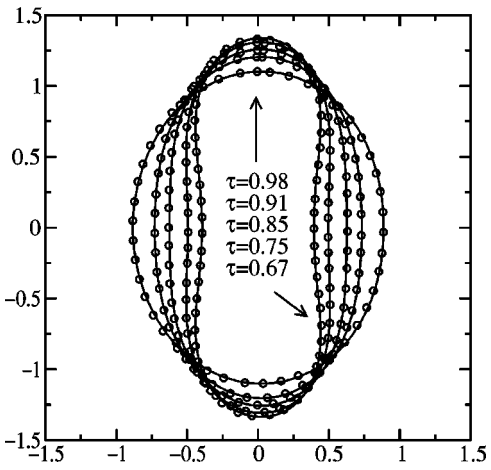

FIG. 22. Equilibrium shapes in two dimensions. Circles correspond to the AF method, while solid lines are the actual contours.

For swelling ratios τ larger than 0.9 the equilibrium shape is reasonably well described by an ellipsis, as can be seen on the figure; however, below that value the comparison becomes poor. For $\tau < 0.85$, indeed, the shape can even become nonconvex (see Fig. 22) and the KS theory can be expected to fail in this region. A direct test of the theory requires the application of an external shear flow, a situation that we consider now.

2. Vesicle in a shear flow

More interesting is the situation where a vesicle is submitted to a shear flow. Such a situation is likely to occur when a vesicle flows in the neighborhood of a wall, a relatively common situation in practice due to sedimentation or confinement. The most basic shear flow to consider is the linear shear flow which is entirely determined by a single parameter γ, the shear rate:

$$v_x = \gamma y,$$

$$v_y = 0.$$

Placed in such a flow, a rigid elongated object is subjected to an angular momentum inducing its rotation (or tumbling motion). However, a vesicle is not a rigid object and when the internal viscosity is identical to the viscosity of the external fluid it has been shown that the vesicle main axis reaches a stationary orientation which is a function of the swelling

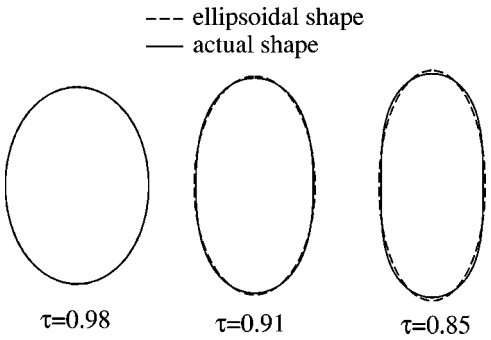

FIG. 23. Comparison in two dimensions of the actual equilibrium shapes with ellipsis.

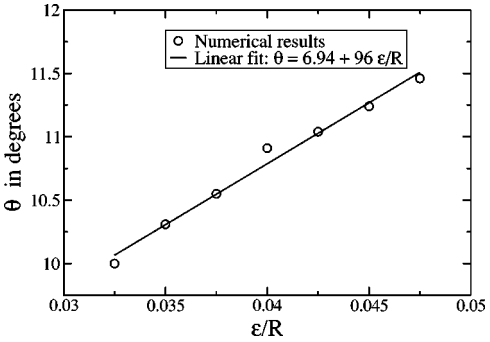

FIG. 24. Variation of θ as a function of the interfacial width ϵ for $\tau=0.8$, $r=4$, and $C_\kappa=0.5$.

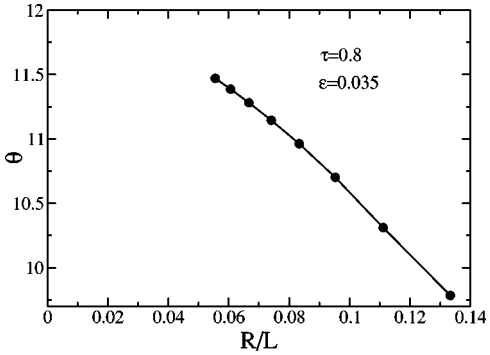

FIG. 25. θ as a function of the inverse box size for $\tau=0.8$, $r=4$, $C_\kappa=0.5$, and $\epsilon=0.035R$.

ratio [16]. If θ denotes the angle between the x axis (shear axis) and the main axis of the vesicle (see Fig. 2), a quasispherical shape would correspond to $\theta=\pi/4$. In general, $\theta<\pi/4$. Although the global shape is stationary, it must be noted that the membrane still circulates along the contour like a tank tread (see Fig. 2).

Interestingly, when the internal viscosity increases up to infinity a transition should occur between the pure tank-treading motion described above and the tumbling motion corresponding to a rigid body. We will use the notation r_c for the critical viscosity ratio at which the transition occurs, which corresponds to the cancellation of θ. Such a transition has indeed been predicted theoretically by Keller and Skalak for red blood cells by assuming ellipsoidal shapes. However, one can easily see from Fig. 22 that in situations corresponding to red blood cells in three dimensions ($\tau\sim0.7$) the shapes are far from ellipsoidal, a careful quantitative analysis of the results is then necessary. It has indeed been shown in Ref. [17] that the AF predictions for the transition location differ from the KS theory. These data were obtained for $\epsilon=0.068R$ and a box size $L=10R$. These two parameters are, however, internal parameters of the resolution method, they are absent from the KS theory that considered a sharp interface and an infinite surrounding medium; the same is true for the Green function formalism, which allows for an exact account of the boundary conditions at infinity. It is then important to compare the AF predictions with the Green function formalism. Here we will analyze both the effect of ϵ, and the finite size effects due to the periodic boundary conditions used in the AF method. In Ref. [17] the finite size effects were considered, assuming that it was the leading source of discrepancy in two dimensions, but the influence of ϵ was not investigated. We will focus first on the influence of ϵ, and to this end consider the tank-treading regime, for which we have a steady state. In Fig. 24 we plot the variations of θ as a function of ϵ for $\tau=0.8$. We can observe a quasilinear dependence of θ as a function of ϵ. An extrapolation to $\epsilon=0$ leads to a value $\theta=6.94$ degrees (the Green function data are 6.2 degrees), whereas for a value of $\epsilon=h$, the minimal resolution, the AF value of θ is around 10 degrees, leading to a strong overestimation of the angle, and therefore of the critical viscosity ratio r_c corresponding to $\theta=0$ [16]. An extrapolation of the AF data to $\epsilon=0$ is thus necessary to obtain quantitative results. Finite size effects due to the chosen periodic boundary conditions can be investigated as well by changing the resolution box size L. Variations of the orientation angle θ, as functions of the inverse box size R/L for $\epsilon=0.035R$ and $\tau=0.8$, are shown in Fig. 25. We observe that the equilibrium angle θ increases with the box size, and the $L\to\infty$ variations thus partially compensate for the $\epsilon\to0$ variations. We can then expect the $\epsilon\to0$, $L\to\infty$ AF prediction for θ to be of the order of 8.5 degrees rather than 6.2 degrees for the boundary integral method. One should not wonder too much about this discrepancy, since we are here in the vicinity of the critical angle $\theta=0$, where a small drift in the control parameters (the swelling ratio for example) can induce dramatic changes in θ. Interestingly, the critical viscosity ratio proves to be rather insensitive to the finite size effects. In Fig. 26 we plot the critical viscosity ratio for $\tau=0.8$ as a function of the inverse box size, and we can see that up to the accuracy of our measurements (the size of the points) we do not observe a significant evolution of r_c. To obtain the transition curve, we can then consider the $\epsilon\to0$ limit only. The extrapolated transition curve is presented in Fig. 5, where r_c have been computed for two values of ϵ and extrapolated to 0.

The crosses correspond to a value $\epsilon/R=0.047$ and the circles to $\epsilon/R=0.035$. An extrapolation to $\epsilon=0$ provides the empty triangles that have to be compared to the results of the boundary integral formulation (the filled triangles). We can observe a fairly good agreement between the extrapolated AF values and the boundary integral reference results. This curve also contains the KS predictions that will be commented upon Appendix D. To conclude this part, the AF

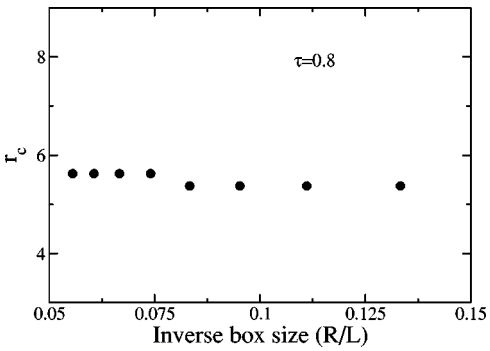

FIG. 26. Evolution of the critical viscosity ratio as a function of the box size.

method is a very good semiquantitative approach that can provide accurate quantitative results if the $\epsilon \to 0$ and $L \to \infty$ limit is carefully investigated. We will mainly use the boundary integral method to test the KS theory, and the AF method to analyze the physical behaviors more qualitatively.

APPENDIX D: DERIVATION OF THE FORCES

1. Derivation of the curvature force

Since the curvature energy is a functional of θ, the curvature force is normal to the membrane and can be written

$$\mathbf{F}_{curv} = -\frac{\delta E_{curv}}{\delta \phi}\frac{\delta \phi}{\delta \mathbf{R}} = 2\frac{\delta E_{curv}}{\delta \phi}\delta^{shape}(\mathbf{r})\hat{\mathbf{n}}. \quad \text{(D1)}$$

The second equality results from Eq. (B8). The functional derivative of E_{curv} can be calculated as usual by doing the transformation $\phi \to \phi + \delta\phi$, which gives

$$E_{curv}[\phi + \delta\phi] = \frac{\kappa}{4}\int\int c^2(\phi + \delta\phi)|\nabla\phi + \nabla\delta\phi|.$$

From the definition $c = -\nabla(\nabla\phi/|\nabla\phi|)$ we easily deduce, in two dimensions

$$\delta c \equiv c(\phi + \delta\phi) - c(\phi) = -\nabla\cdot\left\{\hat{\mathbf{t}}\left(\hat{\mathbf{t}}\cdot\frac{\nabla\delta\phi}{|\nabla\phi|}\right)\right\},$$

from which we obtain after some few integrations by part:

$$\frac{\delta E_{curv}}{\delta\phi} = -\frac{\kappa}{4}\nabla\cdot\left\{c^2\hat{\mathbf{n}} + \frac{\hat{\mathbf{t}}}{|\nabla\phi|}\hat{\mathbf{t}}\cdot\nabla(2c|\nabla\phi|)\right\}. \quad \text{(D2)}$$

To go further, we need to use an important specificity of the advected field, namely that its isocontours are parallel in the interfacial region. This property simply writes $\nabla\cdot\mathbf{t} = 0$. After elementary algebra, using the vectorial identity $(\hat{\mathbf{t}}\cdot\nabla)\hat{\mathbf{t}} = c\hat{\mathbf{n}}$, one can easily obtain

$$\nabla\cdot(c\hat{\mathbf{n}}) = 0,$$

which implies from definition (B7) of the curvature field c that

$$\hat{\mathbf{n}}\cdot\nabla c = c^2,$$

and then the first term appearing in Eq. (D2) simply reduces to $-\kappa c^3/4$.

To calculate the second term, one has to use the basic property $\nabla\wedge\nabla\phi = 0$, which implies, together with $\nabla\cdot\hat{\mathbf{t}} = 0$:

$$\hat{\mathbf{t}}\cdot\nabla|\nabla\phi| = 0.$$

We then obtain the final expression

$$\frac{\delta E_{curv}}{\delta\phi} = -\frac{\kappa}{2}\left\{\frac{c^3}{2} + \hat{\mathbf{t}}\cdot\nabla(\hat{\mathbf{t}}\cdot\nabla c)\right\}, \quad \text{(D3)}$$

which we can combine with expression (D1) to obtain the curvature contribution to the force:

$$\mathbf{F}_{curv} = -\frac{\delta E_{curv}}{\delta\phi}\frac{\delta\phi}{\delta\mathbf{R}} = -\kappa\left\{\frac{c^3}{2} + \hat{\mathbf{t}}\cdot\nabla(\hat{\mathbf{t}}\cdot\nabla c)\right\}\delta^{shape}(\mathbf{r})\hat{\mathbf{n}}.$$

2. Derivation of the Lagrange's force

This force originates from the contribution of the Lagranges parameter to the Hamiltonian of the membrane:

$$E_{Lagranges} = \int\int d\mathbf{r}\zeta\frac{|\nabla\phi|}{2}.$$

An elementary translation leads to the following variation:

$$\delta E_{Lagranges} = \int\int d\mathbf{r}\delta\zeta\frac{|\nabla\phi|}{2} - \int\int d\mathbf{r}\nabla\cdot\left\{\frac{\hat{\mathbf{n}}\zeta}{2}\right\}\delta\phi$$

which, using Eq. (B8), leads to the final expression for the force:

$$\mathbf{F}_{Lagranges} = -\frac{\delta E_{Lagranges}}{\delta\mathbf{R}} = (\hat{\mathbf{t}}\cdot\nabla\zeta\hat{\mathbf{t}} + c\zeta\hat{\mathbf{n}})\delta^{shape}(\mathbf{r}).$$

APPENDIX E: ROLE OF THE COUNTER TERM

The precise role of the counter-term can be understood if we analyze the $\epsilon \to 0$ limit. If r and s denote respectively the normal and the tangential coordinates, the gradient and Laplacian operators can be written

$$\nabla\phi = \frac{\partial\phi}{\partial r}\hat{\mathbf{n}} + \frac{1}{1 - c_0 r}\frac{\partial\phi}{\partial s}\hat{\mathbf{t}},$$

$$\Delta\phi = \frac{\partial^2\phi}{\partial r^2} - \frac{c_0}{1 - c_0 r}\frac{\partial\phi}{\partial r} + \frac{1}{(1 - c_0 r)^2}\frac{\partial^2\phi}{\partial s^2} + \frac{r}{(1 - c_0 r)^3}\frac{\partial c_0}{\partial s}\frac{\partial\phi}{\partial s},$$

where $\hat{\mathbf{n}}$ and $\hat{\mathbf{t}}$ are the normal and tangent vectors, and $c_0(s)$ is the curvature of the zero isocontour of the AF ϕ which has been chosen as the origin of the normal coordinate r [$\phi(r = 0, s) \equiv 0$]. When $\epsilon \to 0$ the width of the interface vanishes and it is therefore convenient to rescale the normal coordinate r by introducing the dimensionless coordinate $r^* = r/\epsilon$. The Laplacian then rewrites

$$\epsilon^2\Delta\phi = \frac{\partial^2\phi}{\partial r^{*2}} - c_0\epsilon\frac{\partial\phi}{\partial r^*} + O(\epsilon^2). \quad \text{(E1)}$$

By definition of the normal vector $\hat{\mathbf{n}} = \nabla\phi/|\nabla\phi|$, ϕ does not vary in the tangential direction ($\partial\phi/\partial s \equiv 0$) so that $|\nabla\phi| = \partial\phi/\partial r \equiv 1/\epsilon\,\partial\phi/\partial r^*$. Equation (E1) can then be rewritten

$$\epsilon^2 \Delta \phi = \frac{\partial^2 \phi}{\partial r^{*2}} - c_0 \epsilon^2 |\nabla \phi| + O(\epsilon^2).$$

An expansion of the curvature field $c(\epsilon r^*, s)$ with respect to ϵ leads to $c = c_0 + O(\epsilon)$, and we can then replace c_0 by c in the previous expression. As a result,

$$\epsilon^2 (\Delta \phi + c|\nabla \phi|) = \frac{\partial^2 \phi}{\partial r^{*2}} + O(\epsilon^2).$$

The role of the counterterm is then to cancel the curvature effects up to the second order in ϵ. As a result, the steady shape of the AF profile is the profile of a flat interface.

[1] P. B. Canham, J. Theor. Biol. **26**, 61 (1970).
[2] W. Helfrich, Z. Naturforsch. A **28c**, 693 (1973).
[3] E. Evans, Biophys. J. **14**, 923 (1974).
[4] F. David and S. Leibler, J. Phys. II **1**, 959 (1991).
[5] U. Seifert, K. Berndl, and R. Lipowsky, Phys. Rev. A **44**, 1182 (1991).
[6] K. Berndl, J. Ks, R. Lipowsky, E. Sackmann, and U. Seifert, Europhys. Lett. **13**, 659 (1990).
[7] J. Ks and E. Sackmann, Biophys. J. **60**, 825 (1991).
[8] L. Miao, U. Seifert, M. Wortis, and H. G. Dbereiner, Phys. Rev. E **49**, 5389 (1994).
[9] Y. C. Fung, *Biomechanics: Mechanical Properties of Living Tissues*, 2nd ed. (Springer-Verlag, New York, 1993).
[10] D. Barthes-Biesel and H. Sgaier, J. Fluid Mech. **160**, 119 (1985).
[11] A. Leyrat-Maurin and D. Barthes-Biesel, J. Fluid Mech. **279**, 135 (1994).
[12] C. Queguiner and D. Barthes-Biesel, J. Fluid Mech. **348**, 349 (1997).
[13] D. Barthes-Biesel, A. Diaz, and E. Dhenin, J. Fluid Mech. **460**, 211 (2002).
[14] C. Pozrikidis, J. Fluid Mech. **440**, 269 (2001).
[15] S. Ramanujan and C. Pozrikidis, J. Fluid Mech. **361**, 117 (1998).
[16] S. R. Keller and R. Skalak, J. Fluid Mech. **120**, 27 (1982).
[17] T. Biben and C. Misbah, Phys. Rev. E **67**, 031908 (2003).
[18] G. B. Jeffery, Proc. R. Soc. London, Ser. A **A102**, 161 (1922).
[19] I. Cantat and C. Misbah, Phys. Rev. Lett. **83**, 880 (1999).
[20] M. Kraus, W. Wintz, U. Seifert, and R. Lipowsky, Phys. Rev. Lett. **77**, 3685 (1996).
[21] U. Seifert and S. A. Langer, Europhys. Lett. **23**, 71 (1993).
[22] I. Cantat and C. Misbah, *Transport versus Structure in Biological and Chemical Systems* (Springer--Verlag, 1999).
[23] I. Cantat, K. Kassner, and C. Misbah, Eur. Phys. J. E **10**, 175 (2003).
[24] R. Folch, J. Casademunt, A. Hernández-Machado, and L. Ramírez-Piscina, Phys. Rev. E **60**, 1724 (1999).